Structural Consequences of Effector Binding to the T State of Aspartate Carbamoyltransferase: Crystal Structures of the Unligated and ATP- and CTP-Complexed Enzymes at 2.6-Å Resolution†,‡

Raymond C. Stevens, J. Eric Gouaux, and William N. Lipscomb*

Gibbs Chemical Laboratory, Harvard University, Cambridge, Massachusetts 02138

Received March 8, 1990; Revised Manuscript Received May 1, 1990

ABSTRACT: The crystal structure of *Escherichia coli* aspartate carbamoyltransferase complexed with adenosine 5′-triphosphate (ATP) has been solved by molecular replacement and has been refined to a crystallographic residual of 0.17 at 2.6-Å resolution by using the computer program X-PLOR. The unit cell dimensions of this crystal form are $a = b = 122.2$ Å and $c = 143.3$ Å and the space group is $P321$. Although the c-axis unit cell dimension is ≈1 Å longer than the corresponding dimension of the CTP-ligated $P321$ crystal form ($c = 142.2$ Å), the ATP-ligated enzyme adopts a T-like quaternary structure. The base moiety of ATP interacts with residues Glu10, Ile12, and Lys60 while the ribose is near Asp19 and Lys60; the triphosphate entity is bound to Lys94, although His20 and Arg96 are nearby. We observe a higher occupancy for ATP in the allosteric site of the R1 regulatory chain in comparison to the occupancy of the R6 allosteric site. These crystallographically independent sites are related by a molecular 2-fold axis. There are other violations of the noncrystallographic symmetry that are similar to those observed in the refined CTP-ligated aspartate carbamoyltransferase structure. These infringements on the molecular symmetry might be the result of intermolecular interactions in the crystal. To ensure the most meaningful comparison with the ATP-ligated structure, we refined the previously reported CTP-bound and unligated structures to crystallographic residuals between 0.17 and 0.18 using X-PLOR. These X-PLOR refined structures are not significantly different from the initial structures that had been crystallographically refined by a restrained least-squares method. After making all possible comparisons between the CTP- and ATP-ligated and the unligated T-state structures, we find that the most significant differences are located at the allosteric sites and in small changes in the quaternary structures. At the allosteric site, the binding of CTP and ATP successively enlarges the nucleotide binding cavity, particularly in the vicinity of the base. The changes in the quaternary structure can be characterized by an increase in the separation of the catalytic trimers by ≈0.5 Å as ATP binds to the unligated T structure. On the basis of these structural studies, we discuss the relationships between the conformational differences in the allosteric site and the small changes in the quaternary structure within the T form to the possible mechanisms for CTP inhibition and ATP activation.

A large part of the biochemical and crystallographic work on allosteric enzymes is focused on aspartate carbamoyltransferase from *Escherichia coli* (also called aspartate transcarbamylase, ATCase; EC 2.1.3.2; Creighton, 1983). ATCase exhibits positive cooperativity toward both substrates in its catalysis of the reaction between carbamoyl phosphate and L-aspartate to give phosphate and *N*-carbamoyl-L-aspartate where the latter product is a precursor in the synthesis of pyrimidines (Jones et al., 1955; Reichard & Hanshoff, 1956). The enzyme, susceptible to feedback regulation, is inhibited by cytidine 5′-triphosphate (CTP), a product of the pyrimidine pathway. Conversely, a product of the parallel purine pathway, adenosine 5′-triphosphate (ATP), stimulates the enzymatic activity. ATCase is a hexamer in both catalytic and regulatory chains (Weber, 1968; Wiley & Lipscomb, 1968); the structure of the holoenzyme consists of two catalytic trimers ($2c_3$) and three regulatory dimers ($3r_2$). Functionally, the catalytic trimers and the regulatory dimers are distinct. The catalytic trimer facilitates the carbamoylation of aspartate by carbamoyl phosphate while the regulatory dimer binds CTP and ATP, but is catalytically inert.

Recent structural studies of ATCase have concentrated on the T[1] → R transition and the catalytic mechanism (Gouaux et al., 1987; Gouaux & Lipscomb, 1988, 1989, 1990). Crystallographic studies on the T-state enzyme ligated with a variety of nucleoside triphosphate molecules proved that ATP and CTP bind to the same site on the regulatory dimer (Honzatko & Lipscomb, 1982), approximately 60 Å from the catalytic active site (Figure 1). However, since the time of those studies, data collection and crystallographic refinement can be carried out more accurately and more rapidly, and we report here the results of such studies.

The apparent separation of the homotropic cooperativity induced by the substrates from the allosteric inhibition and

†This work was supported by National Institutes of Health Grant GM06920 (W.N.L.) and a National Institutes of Health postdoctoral fellowship (R.C.S.).

‡The coordinates for the structures have been deposited in the Brookhaven Protein Data Bank under entry names 4AT1, 5AT1, 6AT1, 7AT1, and 8AT1.

[1] T is an abbreviation for tense and is used here to indicate the conformational state of the enzyme that has unit cell dimensions of $a = 122$ Å and $c = 142$ Å in the space group $P321$; R, an abbreviation for relaxed, indicates the conformational state of the enzyme that has unit cell dimensions of $a = 122$ Å and $c = 156$ Å also in the space group $P321$. Functionally, the T form usually shows low activity and low aspartate affinity while the R form has a high activity and a high affinity for aspartate. See Monod et al. (1965) for a discussion on a theory of allosteric transitions in proteins and for an explanation of the nomenclature.

0006-2960/90/0429-7691$02.50/0

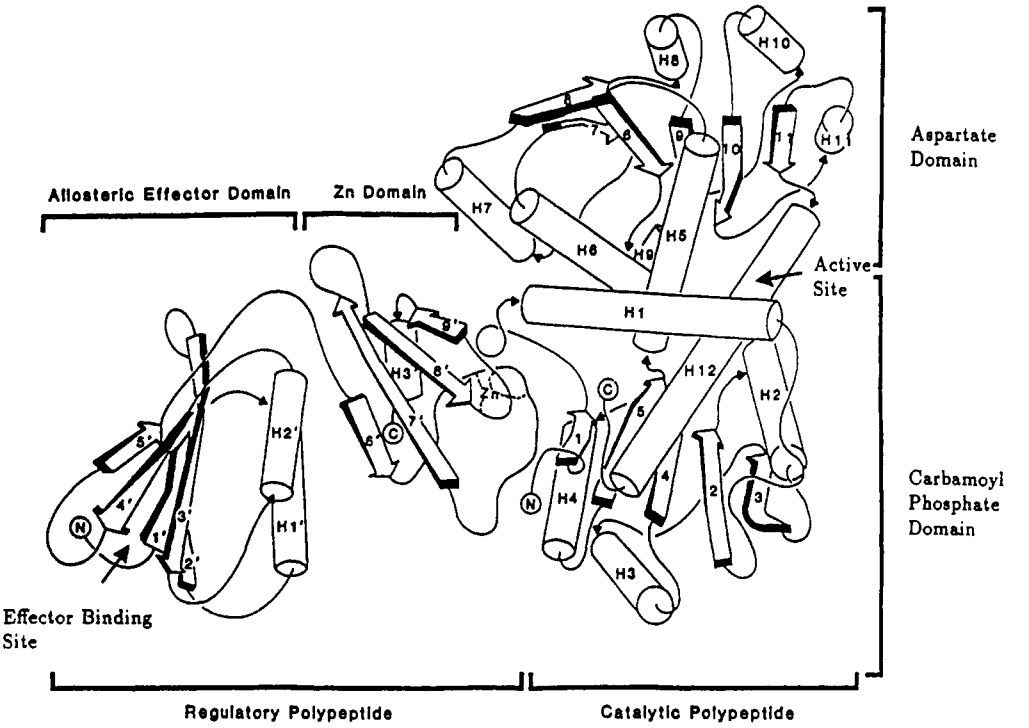

FIGURE 1: View of one catalytic–regulatory pair illustrating the 60-Å pathway between the allosteric domain (left) and the active site (right). The asymmetric unit is composed of two of these catalytic–regulatory pairs.

activation caused by CTP and ATP has been illustrated in a number of instances. In the presence of the aspartate analogues L-cysteinesulfinate (Foote & Lipscomb, 1985) or L-alanosine (Baillon et al., 1985), the activity of the native enzyme can be stimulated by ATP and inhibited by CTP. These substrate analogues do not elicit homotropic cooperativity, and the dominant part of the catalysis probably occurs on enzyme molecules that are in a T-like state. Nevertheless, CTP and ATP can still modulate the enzyme's activity. One interpretation of these results is that ATP and CTP do not directly perturb the T $\rightleftharpoons$ R equilibrium but rather they alter the enzyme's affinity for aspartate, which then may change the equilibrium between the T and R states. However, equilibrium dialysis experiments indicate that the effects of ATP or CTP binding to the native enzyme are strictly coupled to the T and R equilibrium (Newall et al., 1989). In order to provide a structural basis for the mechanism of ATP activation and CTP inhibition on enzyme molecules in the T state, we have determined the structure of aspartate carbamoyltransferase ligated with ATP. We have also compared this structure with the T-state structures of the unligated and CTP-complexed enzymes. On the basis of the structural differences between these enzyme models and on the results from kinetic, thermodynamic, and biochemical experiments, we suggest mechanistic hypotheses for the heterotropic cooperativity of ATCase.

Materials and Methods

Materials. Maleic acid (MCB Reagents), Tris-HCl (BRL), 2-mercaptoethanol, ATP (Sigma), EDTA (J. T. Baker), sodium azide (Kodak), sodium hydroxide (Fisher), and poly(ethylene glycol) 8000 (Fluka) were all used without further purification. Wild-type aspartate carbamoyltransferase was isolated as described (Nowlan & Kantrowitz, 1985) from the EK1104 strain of *E. coli*, which contained the plasmid pEK2 carrying the entire native *pyr*BI operon, in the laboratory of E. R. Kantrowitz at Boston College.

(*a*) T^{atp}[2] *Crystallization, Data Collection, and Refinement.* Crystallization was effected by dialyzing the enzyme solution at room temperature against a buffer of 100 mM maleic acid, 10 mM Tris-HCl, 1 mM 2-mercaptoethanol, 0.2 mM EDTA, and 0.3 mM NaN_3, pH 5.7, with NaOH. The protein concentration was 6 mg/mL, as determined at A_{280} with an extinction coefficient of 0.59 cm^2/mg (Gerhart & Holoubek, 1967) for the holoenzyme. Typically, hexagonal plates in the space group *P*321 ($a = b = 122.2$ Å, $c = 142.2$ Å) grew in 1–2 weeks. Crystals were then soaked in the above buffer with an additional 2.5 mM ATP and 10% poly(ethylene glycol) 8000. When higher concentrations of effector were employed or when the pH was increased, the crystals dissolved or cracked. It has been shown by Gouaux and Lipscomb (1990) that substrate-analogue-complexed ATCase obtained via soaking or cocrystallization and pH 5.8 or pH 7.0 yields similar structures.

Data were collected to 2.5-Å resolution on the multiwire proportion chamber at the University of Virginia (Sabottka et al., 1984). Three T^{atp} crystals were used in the data collection; all three displayed a slightly longer *c*-axis ($c = 143.3$ Å) in comparison to the same crystals ($c = 142.2$ Å) before treatment with the ATP soaking buffer and in comparison with results in earlier reports of the T-state crystals ($c = 142.2$ Å) (Kim et al., 1987). The crystal to detector distance of 112.0 cm was chosen to maximize the density of reflections measured on each detector and to minimize the number of overlapping reflections. Helium boxes were placed between the crystal and detector to minimize signal attenuation due to scattering from air. The asymmetric unit of reciprocal space was measured by fixing ϕ and χ and sweeping ω through values determined with the program LATTICEPATCH (Klinger & Kretsinger, 1989) on a Silicon Graphics IRIS Series 3000 computer.

[2] To signify that a structure contains a ligand bound at the active site, we will add an abbreviation of the ligand name as a subscript to either T or R. Alternatively, if the ligand is bound to the regulatory site, then an abbreviation for that ligand will be added as a superscript. For example, the abbreviation for the T-state enzyme ligated with ATP would be T^{atp}.

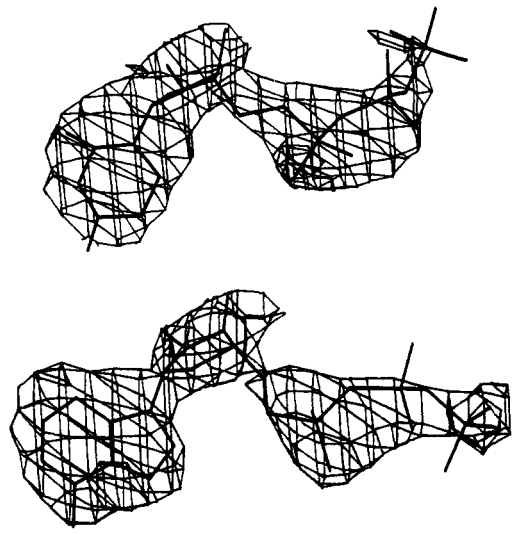

FIGURE 2: Electron density of CTP (top) and ATP (bottom) in the upper allosteric domain. Electron density is at approximately 3σ for each map. The electron density for the lower allosteric domains is much weaker (approximately 1.5σ).

In this manner, 74676 reflections were measured on three crystals with an average exposure time of 20 h for each crystal. The intensities were integrated and then corrected for Lorentz and polarization factors. According to the method of Fox and Holmes (1966), the data were reduced to 25297 independent reflections yielding an R_{merge} [$R_{merge} = \sum_{hkl}(\sum_i|I - \bar{I}|/\sum_i I)$] of 4.6%. Crystallographic refinement proceeded by using data between 10 and 2.6 Å with 23826 unique reflections.

The crystal structure was solved by using the molecular replacement method, employing the T^{ctp} structure of Kim et al. (1987) as the initial model, with a beginning R-factor of 0.28. After several cycles of rigid body refinement, simulated annealing was employed followed by Powell minimization using the program X-PLOR (Brünger et al., 1987) on the Cray YMP computer at the Pittsburgh Supercomputer Center. Electron density maps were calculated by using coefficients of $(F_o - F_c)$ and $(2F_o - F_c)$. These maps were carefully compared with the refined protein structure by utilizing the computer program FRODO (Jones, 1982) in a modified form (Pflugrath et al., 1984) on an Evans and Sutherland PS300 graphics system interface to a VAX 11/780 computer. Initially, only one ATP molecule was clearly located in the $(F_o - F_c)$ map at the 3σ level (Figure 2); a second ATP molecule was later located in the lower regulatory chain (R6) at the 1.3σ level. The model of ATP derived from a small-molecule structure determination (Kennard et al., 1971) was then built into both regions of the electron density assigned to ATP. Only minor changes to the torsion angles were required to fit the models to the electron density. In Figure 3 we illustrate the atomic nomenclature for both ATP and CTP. At the active site, which cannot accommodate the entire nucleoside triphosphate molecule, we observe a few electron density peaks near the center of the active site at the 2σ level. These peaks appear in both catalytic sites of the crystallographic asymmetric unit, and we suspect that they are due either to the γ-phosphate groups of mostly disordered ATP and CTP or more probably to solvent molecules. No solvent molecules have been included in the refinment.

The following criteria were used to assess the accuracy of the protein coordinates. (i) The standard deviations of the electron density were calculated for all of the electron density maps. (ii) The most well ordered elements of the secondary structure were selected for comparison with the electron density

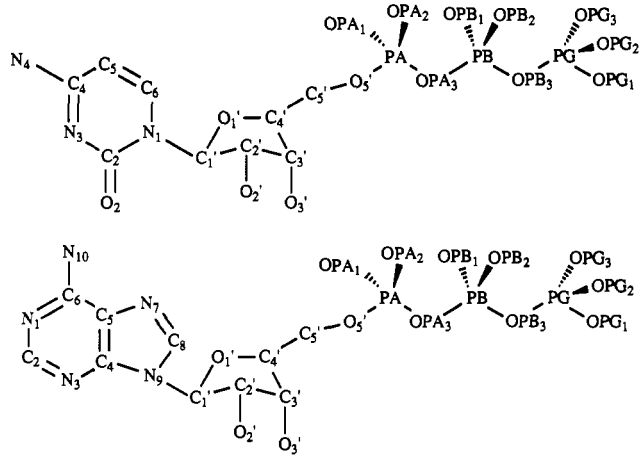

FIGURE 3: Molecular structure and numbering scheme of CTP (top) and ATP (bottom).

Table I: Secondary Structural Definitions for Aspartate Carbamoyltransferase

secondary element[a]	residue span of element	secondary element[a]	residue span of element
	Carbamoyl Phosphate Domain		
S1	7–9	S4	101–106
T1	11–14	H4	111–119
H1	17–32	S5	123–127
S2	42–48	T2	129–132
H2	53–66	H5[b]	135–149
S3	68–74	H12[b]	285–305
H3	88–98		
	Aspartate Domain		
H5[b]	135–149	S9	224–230
S6	155–160	H9	237–242
H6	167–179	H10	251–256
S7	182–188	S10	262–265
T3	189–192	H11	275–279
H7	196–205	S11	281–283
S8	208–212	H12[b]	285–305
H8	215–220		
	Allosteric Domain		
S1′	14–19	H2′	69–77
H1′	25–33	S4′	82–87
S2′	41–46	S5′	93–97
S3′	55–62		
	Zinc Domain		
S6′	102–104	S9′	143–146
S7′	123–129	H3′	147–150
S8′	135–138		

[a] H, α-helix; S, β-strand; T, reverse turn. [b] H5 and H12 connect the carbamoyl phosphate domain to the aspartate domain.

maps (Table I). For both main-chain and side-chain atoms, the height of the associated electron density peaks was determined by the number of standard deviations above background. (iii) The overall structure was analyzed, and electron density regions below that of the "ordered" regions were noted as disordered. (iv) Those areas that were in "weak" density were carefully examined and a best fit was made of the atoms of the protein to the electron density.

Disorder at particular sites acts as an excellent indicator of flexibility within the protein structure. The determination of information regarding disorder can yield valuable information relating to activity and allosteric regulation. Specifically, residues 75–86 (80s loop) and 239–247 (240s loop) in the catalytic chains were found to be disordered; both are flexible regions of the protein. Of course, nonfunctional disorder may also be present. In the regulatory chain the electron density is of lower quality in the regions 8–11, 49–55,

Table II: Data Collection Parameters for ATCase–Effector Crystallographic Studies

structure[a]	unit cell (Å)	resolution (Å)	reflections collected	unique reflections	R_{merge} (%)[b]
unligated	a = 122.2, c = 142.2	2.6	78896	26912	~6.0
T^{atp}	a = 122.2, c = 143.3	2.6	74676	25297	4.6
T^{ctp}	a = 122.2, c = 142.2	2.6	~113912	23334	~6.0

[a] All structures are in the space group $P321$, No. 150. [b] $R_{merge} = \sum_{hkl}(\sum_i|I - \bar{I}|/\sum_i I)$.

Table III: Refinement Parameters for ATCase–Effector Crystallographic Studies[a]

structure	R_{factor}[b]	root mean square deviation[c]	noncrystallographic symmetry[d] (Å)
unligated	0.18	0.016 Å, 3.5°	0.5 C, 1.3 R
T^{atp}	0.17	0.014 Å, 3.4°	0.5 C, 1.2 R
T^{ctp}	0.17	0.015 Å, 3.5°	0.5 C, 1.2 R

[a] Solvent molecules have not been included in the refinement. [b] $R_{factor} = \sum_{hkl}(||F_o| - |F_c||/|F_o|)$. [c] The rms deviations of bond lengths and three atom bond angles from the corresponding parameters contained in version 1.5 of X-PLOR. [d] C, catalytic chain; R, regulatory chain, all non-hydrogen atoms.

87–90, and 130–133. These regions of electron density were definitely traceable but were not as strong as density in the other parts of the structure. Refinement was considered complete once no further movement in the regions could be detected when compared to a standard structure, initially unligated ATCase. This refinement required approximately 500 cycles of Powell minimization. Toward the end of the refinement, simulated annealing was employed to locate possible alternate conformations within the structure. Final data collection and refinement statistics are given in Tables II and III, respectively.

(*b*) T^{ctp} *Refinement*. The results of the T^{atp} refinement were used in the T^{ctp} analysis with the original 23 334 reflections (Kim et al., 1987). We used the program X-PLOR (Brünger et al., 1987) and compared the results to those of the earlier study which employed the program PROLSQ (Konnert & Hendrickson, 1985). Data collection statistics and refinement factors are given in Tables II and III. The refinement proceeded smoothly, except for regions 76–83 and 243–245 in the catalytic chains and residues 8–10, 50–54, 87–91, and 130–133 in the regulatory chain. In agreement with the original report of this structure (Kim et al., 1987), we find the first CTP molecule to be approximately 3σ above background and the second CTP molecule at the 1.3σ level. The refined structure was not significantly different from that reported by Kim et al. (1987). Simulated annealing was employed to locate possible alternate conformations. At the active site, a few peaks were observed which we suspect to be water molecules similar to the peaks located in the T^{atp} structure.

(*c*) *T (Unligated) Refinement*. The structure derived from the T^{atp} and T^{ctp} refinements was used in the refinement of the unligated enzyme employing the original 26912 reflections (Ke et al., 1984). Data collection statistics and refinement factors are given in Tables II and III. The refinement proceeded smoothly, except for regions 76–83 and 243–245 in the catalytic chains and residues 8–10, 50–54, and 87–91 in the regulatory chain. The active site of the unligated enzyme showed nonprotein peaks at positions noted above in the T^{atp} and T^{ctp} structures. Simulated annealing was again employed to locate possible alternate conformations.

All three structures were refined by using Powell minimization, followed by model building, simulated annealing, and, finally, several cycles of Powell minimization and *B*-factor refinement. Stereochemical restraints consisted of the default bond, angle, torsion, improper, and van der Waals energy functions as defined in version 1.5 of X-PLOR (Brünger, 1988). Bond lengths and angles for the zinc–sulfur interactions in the regulatory chain were derived from the crystal structure of a small molecule (Swenson et al., 1978). These values for the zinc–sulfur bond lengths are in agreement with the average values as determined from EXAFS experiments on aspartate carbamoyltransferase (Philips et al., 1982). The force constants on the bond and angle terms were empirically adjusted to maintain an appropriate tetrahedral geometry. To avoid biasing the model by including Coulombic energy functions, all charges on the ligand atoms and side-chain groups of Asp, Glu, Arg, Lys, and His were turned off during the refinement.

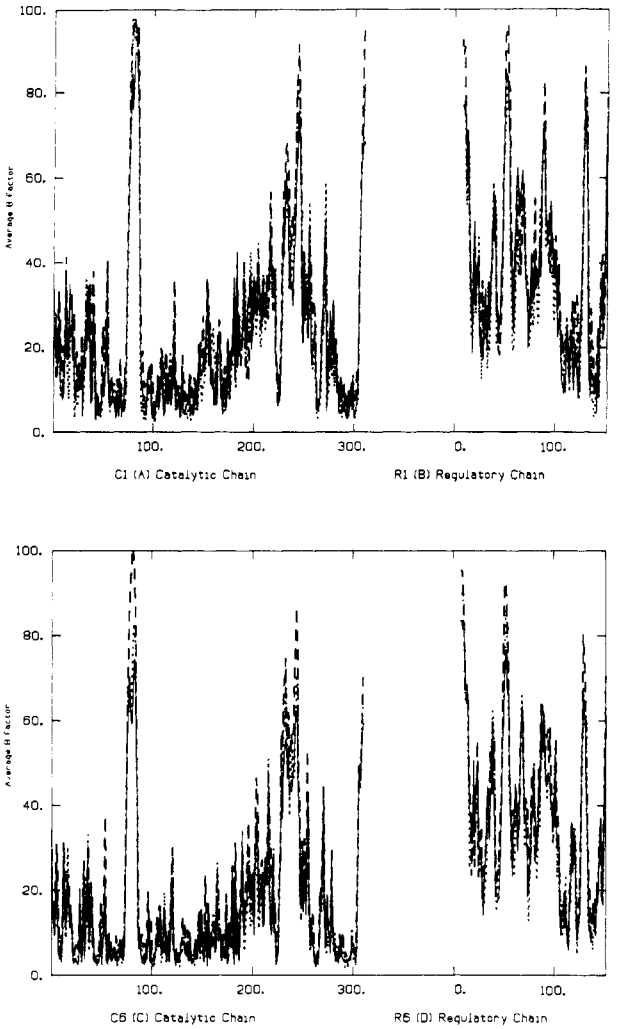

FIGURE 4: Plot of average *B*-factor (Å^2) vs residue number for both catalytic and regulatory chains. The top graph is the upper C1,R1 chains of the asymmetric unit and the bottom graph the C6,R6 chains. Unligated structure is represented by a solid line, T^{atp} by a dashed line, and T^{ctp} by a dotted line.

RESULTS

(*a*) *Comparison of Electron Density*. All three structures display similar regions of strong and weak density and average *B*-factors for each of the four polypeptide chains (unligated, 22.0, 37.4, 15.7, and 35.9 Å^2; T^{atp}, 24.6, 39.6, 19.3, and 39.6 Å^2; T^{ctp}, 21.9, 36.0, 16.3, and 35.9 Å^2 for C1R1–C6R6 chains, respectively, which define the asymmetric unit). The average *B*-factors are plotted against the residue numbers in Figure 4. These *B*-factors are known to indicate errors in atomic

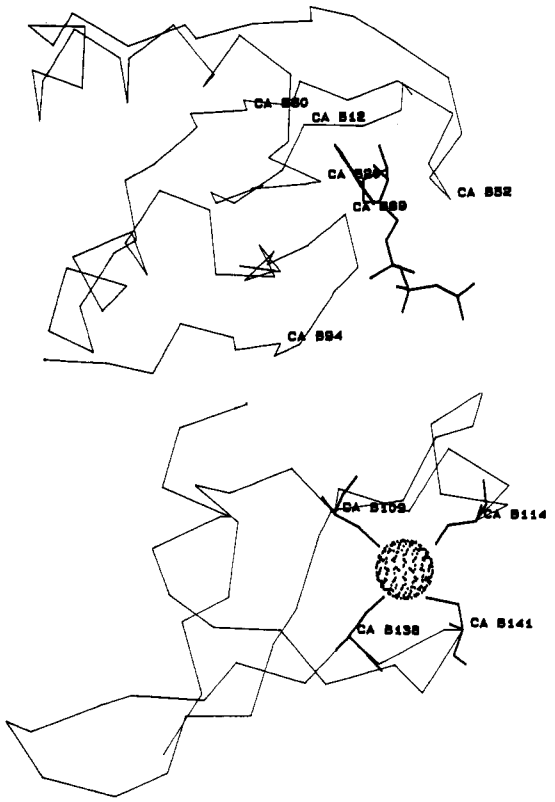

FIGURE 5: (Top) Effector binding cavity (C_α trace) where both ATP and CTP are observed to bind in identical locations. (Bottom) Zinc binding site in the regulatory chain bound by four cysteine residues (residues 109, 114, 138, and 141).

positions as well as regions of high mobility (Kuriyan et al., 1987).

Both catalytic chains are observed to have particularly high *B*-factors for the 80s loop (residues 75–85), a general increase in average *B*-values between residues 140–280 (aspartate domain), and a strong increase in the 240s (235–245) loop which is crucial in the T to R transition (Kantrowitz & Lipscomb, 1988, 1990). The 80s loop was found in extremely weak density. However, the trace of the protein structure is not in doubt in this region because this 80s loop is well-defined in the electron density of the R state (Ke et al., 1988). The general increase of *B*-values for residues 140–280 in the aspartate domain (Figure 1) occurs for residues at an interface to the zinc domain of the corresponding regulatory chain, between neighboring catalytic chains, or on the surface of the hexameric structure. These results are in contrast to the *B*-values of the carbamoyl phosphate domain, which is buried within the hexamer. The upper catalytic chain (C1) has a slightly higher average *B*-factor (by approximately 6 Å^2) than its noncrystallographically related lower catalytic chain (C6) in all three structures. This differential effect did not occur in the noncrystallographically related regulatory chains.

Within the regulatory chain, residues 1–7 have been omitted as in earlier studies (Kim et al., 1987; Ke et al., 1988) of the T and R forms due to a lack of density, even though the effectors ATP and CTP are located in close proximity to the plausible locations for these residues. The effector and zinc binding sites within the allosteric and zinc domains are shown in Figure 5. The average *B*-factor of the regulatory chain is much higher than that of the catalytic chain. Moreover, the allosteric domain has a higher average *B*-factor than the zinc domain. Some regions are exceptions, for example, the 130s loop of the zinc domain. Within the allosteric domain high values are seen in residues 8–20. A complete rebuilding of this region, however, yielded confirmation of the original trace of the polypeptide chain. The other regions with high *B*-factors in the regulatory chain are the 50s, 90s, and 130s loops. The former two loops are found to connect β-strands which define the β-sheet composed of S1′–S5′ of the allosteric domain, in close proximity to the effector binding site. the 130s loop makes an intermolecular interaction with the 90s loop of a neighboring allosteric domain in an adjacent molecule in the crystal structure. This interaction is stronger in the T^{atp} and T^{ctp} structures than in the unligated structure. Additionally, Arg130 is found to interact with an oxygen from the γ-phosphate of ATP. The latter interaction occurs only in the upper regulatory chain and may be sensitive to pH.

The estimate of the coordinate error of ~0.5 Å was based on the multiple refinements of the initial coordinates and on Luzzati plots (Luzzati, 1952). This value agrees well with previous reports on the accuracy of the coordinates for ATCase (Kim et al., 1987; Ke et al., 1988).

(*b*) *Movement of Domains.* On the basis of our previous X-ray diffraction results and on the previous reports from X-ray solution scattering (Hervé et al., 1985) and sedimentation velocity (Werner & Schachman, 1989), large movements of polypeptide chains (catalytic and regulatory) and domains (carbamoyl phosphate, aspartate, allosteric, zinc; see Figure 1) were not expected within the T quaternary structure. To analyze the movement in domains, the C_2R_2 units were superimposed upon one another, then each polypeptide chain was superimposed, and finally each domain was superimposed. We remind the reader that in the T → R structural transition, the two C_3 units move apart by 12 Å and reorient about the molecular 3-fold axis by ±5°, and the regulatory dimers reorient about the molecular axes by 15° in a way that preserves the CRRC interactions. These superpositions show, upon comparison of the T^{atp} to the unligated structure, an increase in the C_3 trimer separation of 0.5 Å. This separation distance is small but significant. Owing to the large number of atoms involved, the estimated standard error is roughly 0.01 Å.[3]

(*c*) *Movement of Residues.* The general procedure in the analysis of the movement of residues was initiated by superimposing the C_α trace of the complete C_2R_2 unit in two holoenzyme structures being compared, followed by the calculation of a root mean square (rms) deviation between coordinates of these two structures. All three structures were found to be similar, with an overall average rms displacement of 0.4 Å (non-hydrogen atoms) for the catalytic chains and 1.2 Å (non-hydrogen atoms) for the regulatory chains. When superposition was applied to individual domains, the differences decreased. This decrease may be partly associated with the intrinsic or crystallization-induced asymmetry of the C_2R_2 unit (Kim et al., 1987). In order to maximize information at the domain level, we superimpose the C_2R_2 unit in our comparison and also superimpose separately the individual domains.

As expected, movements in the side chains in these comparisons of the T^{atp} and T^{ctp} structures to the unligated structure were larger than for the backbone. The average rms displacement values are 0.4 Å for the catalytic chains and 1.4 Å for the regulatory chains. These differences may be attributed to several factors including multiple conformations, weak electron density, and movement of residues due to effector binding. No obvious movement of residues that could be attributed to the effector binding was observed, although

[3] Standard error of the mean = $\sigma/\sqrt{n}$ for large n, where n = 1860 C_α atoms and σ = 0.5 Å (based on the Luzatti plot and comparison between similar structures). The standard error is correlated with the *c*-axis unit cell dimension.

Table IV: ATP Binding Site Interactions[a]

ligand atom	protein atom[b]	distance[c] (Å)	ligand atom	protein atom[b]	distance[c] (Å)
$C_{2'}$	Val9 O	3.0/4.1	$O_{2'}$	Lys60 NZ	2.7/3.2
$O_{2'}$	Val9 O	2.9/2.7	N_3	Lys60 CE	3.4/3.0
N_3	Glu10 O	3.8/2.9	N_3	Lys60 NZ	3.0/2.2
C_2	Glu10 C	3.4/3.2	OPA_1	Asn84 OD1	3.5/4.1
C_2	Glu10 O	3.3/3.0	N_{10}	Tyr89 O	2.6/3.0
N_1	Ala11 CA	2.4/2.8	OPA_1	Val91 CG1	3.2/4.5
N_1	Ala11 C	2.9/3.1	OPA_1	Val91 CG2	2.9/4.0
C_2	Ile12 N	3.3/3.2	PB	Lys94 NZ	3.2/4.2
N_1	Ile12 N	2.6/2.6	OPB_2	Lys94 NZ	2.7/4.5
N_{10}	Ile12 O	3.4/3.4	OPB_1	Lys94 CE	2.5/3.5
$O_{3'}$	Asp19 OD1	2.6/4.9	OPB_1	Lys94 NZ	3.1/3.3
$O_{3'}$	Leu58 CD1	3.5/3.5	OPA_1	Lys94 NZ	3.6/2.4

[a] The atoms are designated according to the labels given in Figure 3. Interactions are defined as contacts less than 3.8 Å. Nonpolar interactions are included that may be responsible for steric effects. [b] The protein atoms are those of standard convention in version 1.5 of X-PLOR (Brünger, 1988). [c] Upper regulatory chain/lower regulatory chain ATP interactions.

Table V: CTP Binding Site Interactions[a]

ligand atom	protein atom	distance (Å)	ligand atom	protein atom	distance (Å)
N_4	Ile12 O	3.0/2.0	OC_2	Lys60 NZ	2.7/2.2
$O_{3'}$	Val17 CG1	2.8/4.9	$O_{5'}$	Asn84 OD1	3.5/3.6
OC_2	Val17 CG2	2.9/3.5	N_4	Tyr89 O	3.3/3.9
$C_{3'}$	Asp19 OD2	3.4/3.7	PA	Val91 CG2	3.4/3.9
$O_{3'}$	Asp19 CG	3.2/3.7	OPA_1	Val91 CG2	3.0/3.9
$O_{3'}$	Asp19 OD2	3.0/2.6	$O_{5'}$	Val91 CG2	3.1/3.1
$O_{2'}$	Lys60 NZ	2.5/3.3	OPB_1	Lys94 CE	3.2/5.8
C_2	Lys60 NZ	3.7/3.2	OPB_1	Lys94 NZ	3.2/5.2
OC_2	Lys60 CD	3.1/3.7	OPA_2	Lys94 CE	2.4/3.2
OC_2	Lys60 CE	3.2/2.5	OPA_2	Lys94 NZ	2.7/2.2

[a] Conventions identical with those employed in Table IV are used in this table.

the C1–C4 interface contacts were found to be longer in the T^{atp} structure as compared with the T^{ctp} and unligated structures. These longer contacts could facilitate the movement of the 240s loop when the second substrate (Asp) binds and may increase the affinity for aspartate.

(*d*) *Comparison of Effector Binding Sites.* Listed in Tables IV and V are the ATP and CTP binding site interactions, respectively. All polar and nonpolar contacts less than 3.5 Å are listed. Figures 6–8 display the similarities in binding site for ATP and CTP. In agreement with past crystallographic studies (Honzatko et al., 1979; Honzatko & Lipscomb, 1982a,b), ATP and CTP bind in the same location of the allosteric domain (Figure 6) and they are bound by similar residues. Both effectors also display similar occupancies in the upper and lower chains of 0.7 and 0.3 $Å^3$, respectively, based on a comparison with well-defined residue occupancies. Incorporation of ATP or CTP into the unligated structure shows an expansion of the effector binding site upon binding of the nucleotides. Moreover, ATP expands the cavity slightly more than does CTP. The most apparent movements within the cavity are residues Ala11 and Ile12, which are located near the beginning of the S1′ β-strand, and Glu90, which does not directly interact with the nucleoside triphosphates but moves more than 2 Å as shown in Figures 7 and 8. Movements of residues, particularly Lys94, near the triphosphate moiety of the effectors are also observed. Unacceptably close interactions were observed when ATP was modeled in place of CTP in the T^{ctp} structure. The triphosphate moieties for the ATP and CTP molecules are found to be in slightly different conformations, however; both triphosphate moieties are slightly disordered, particularly the γ-phosphate. Studies of the effects of pH on this disorder may be useful.

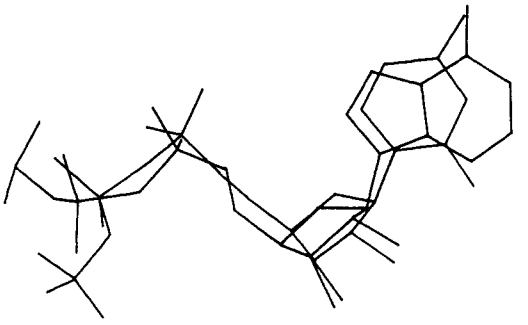

FIGURE 6: ATP and CTP are found to bind in almost identical sites as illustrated above in which the molecules were plotted after superpositioning of the C_α trace of the CR dimer.

Discussion

Our present study concerns the heterotropic cooperativity of *E. coli* aspartate carbamoyltransferase. Functionally, ATP and CTP manifest their effects by shifting the position of the $[S]_{0.5}$ for aspartate to lower and higher concentrations of aspartate, respectively. Several models have been proposed to account for the effects of ATP and CTP. Proponents of one model state that the nucleoside triphosphates simply shift the equilibrium between the T and the R states (Monod et al., 1965; Schachman, 1988). Advocates of another model postulated that ATP and CTP do not directly influence the T and R equilibrium but rather that they exert a primary effect which changes the enzyme's affinity for aspartate, regardless of the quaternary state; the change in the strength of aspartate binding can then perturb the balance between the different quaternary states, giving rise to a secondary effect (Hervé, 1989). A third model, developed by Wedler and co-workers, is based on equilibrium isotope-exchange studies. Their hypothesis is that ATP and CTP do not act on the T to R state transition but rather they change the rate of aspartate association (Hsuanyu & Wedler, 1988). In this and the following paper we provide a structural basis for a discussion of the different allosteric mechanisms of aspartate carbamoyltransferase.

There are several circumstances in which the homotropic cooperativity evoked by the substrates apparently can be "disconnected" from the heterotropic effects caused by ATP and CTP (Foote et al., 1985; Baillon et al., 1985), although this conclusion has been contested (Schachman, 1988). These results and conclusions, in part, provide a motivation for experiments to determine the structural consequences of ATP and CTP binding to the T-state enzyme. From our analysis of the structures of the T-state enzyme in the absence of substrates or substrate analogues, we observe that ATP alters the quaternary structure; ATP shifts the structure in the direction of the R state, increasing the separation of the catalytic trimers. Coupled to the small quaternary conformational changes are slight differences in the C1:C6 interfaces; however, there are no large conformational changes at any interfaces. Consistent with previous studies on the effect of ATP and CTP to the enzyme in the absence of active-site ligands, we find that ligation of the enzyme with ATP is not sufficient to promote large movements of the catalytic trimers and regulatory dimers or the T → R transition. Nevertheless, how might the binding of ATP and CTP to the allosteric site produce small but significant changes in the quaternary structure?

Four main areas were focused on in comparing the three structures: (i) differences within the effector binding site, (ii) movement of residues, (iii) differences between interface contacts, and (iv) movement of domains. Our detailed de-

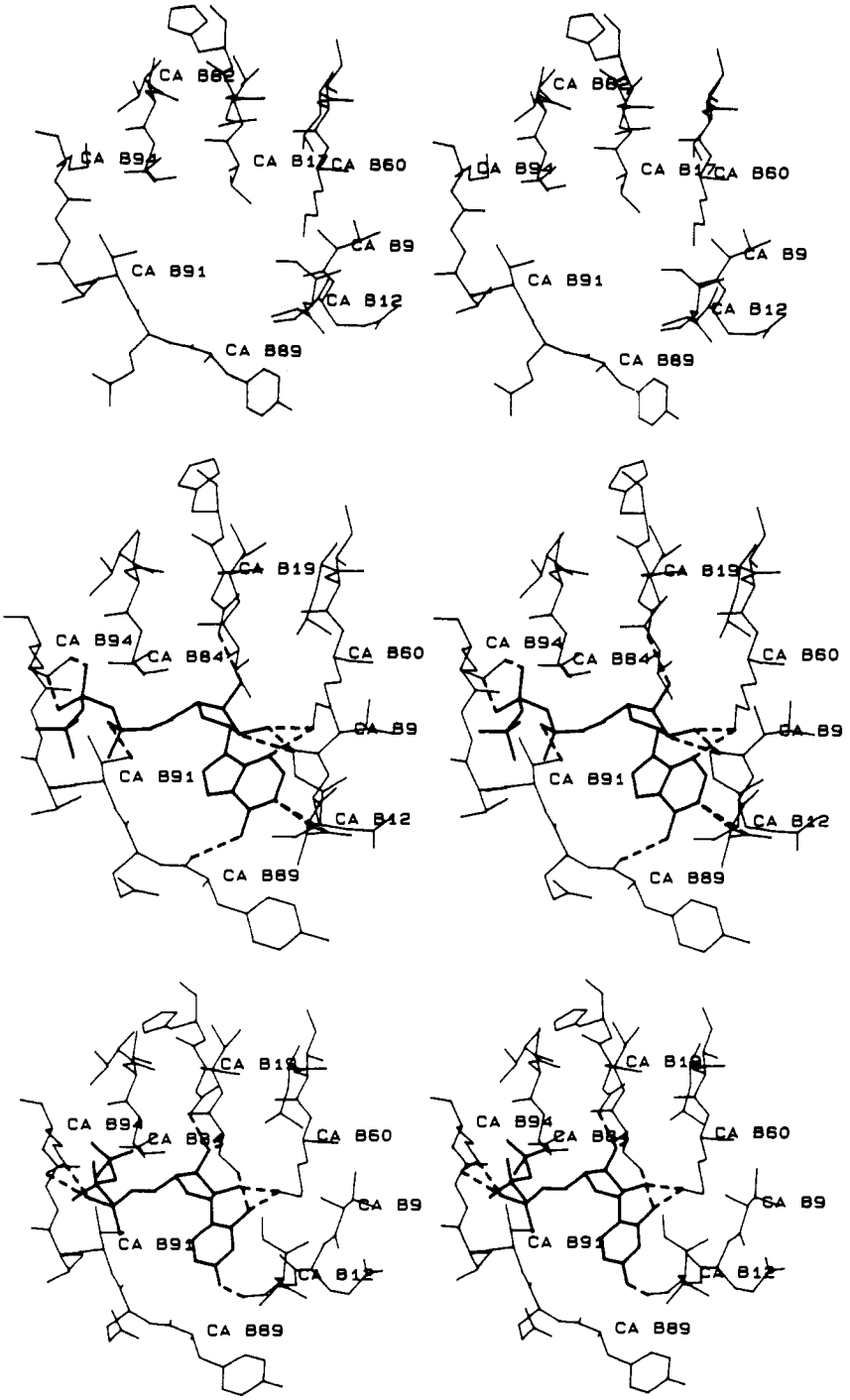

FIGURE 7: CPK model with backbone atoms of the effector binding clefts. The side chain of Ile12 has been removed from each figure for clarity; it is observed to bind over the top of the base for each nucleotide. Unligated (top), ATP (middle), and CTP (bottom) effector binding sites.

scription of binding of nucleotides is consistent with the schematic model suggested by London and Schmidt (1972), modified to omit metal ion in the nucleotide–enzyme interaction in agreement with conclusions of Rosenbusch and Weber (1971). We see no evidence for binding of nucleotides at the active site. Our observation of three higher and three lower occupancy sites in the six regulatory chains is consistent with negative cooperativity of nucleotide binding (Matsumoto & Hammes, 1973). Unfortunately, because of the intermolecular interaction of the three strong sites, we are not able to offer our evidence in support of this negative cooperativity, although our results are at least consistent with this conclusion. Moreover, we are not able to distinguish between the preexistence of two classes of sites before nucleotide binding as compared with the creation of a second class of sites by the binding of the nucleotides to the first three sites (Tondre & Hammes, 1974).

Both the purine and pyrimidine rings are found to be located in very similar locations, as are the ribose rings. The main difference is that the T^{atp} nucleotide binding cavity is expanded slightly more than the T^{ctp} nucleotide cavity, and both are found to be much larger than the unligated binding site. This expanded site in the T^{atp} structure displaces the S1′ β-strand sufficiently that the ribose and triphosphates of the ATP and CTP can bind in the same regions of the regulatory site of the enzyme (induced fit). Val9r and Glu10r are found to move inward toward ATP in the T^{atp} structure, while in the T^{ctp} structure they are not observed to move. This result may relate

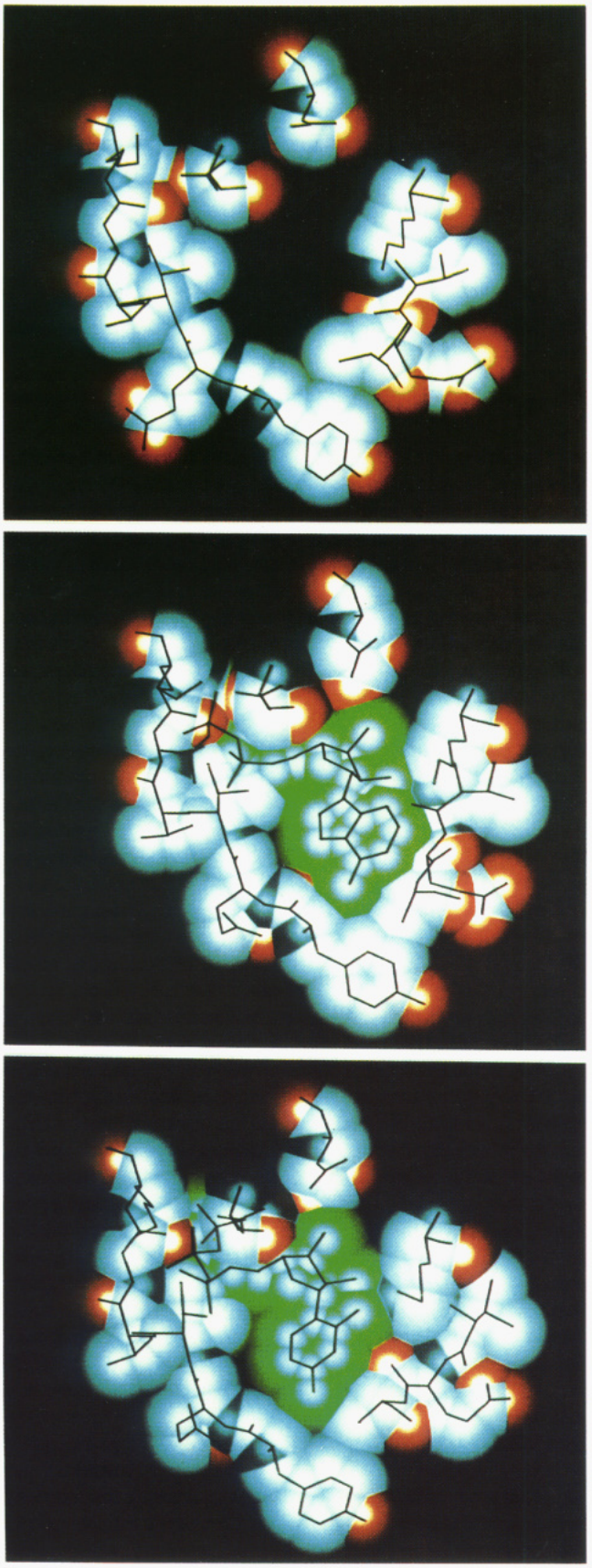

FIGURE 8: Stereoview of the unligated (top), ATP (middle), and CTP (bottom) effector binding sites which complements Figure 7. Note the increase in cavity size upon complexation with the effectors ATP and CTP. All residues listed in Tables IV and V are shown; only those interactions within 3.0 Å of the nucleotides are drawn with broken lines.

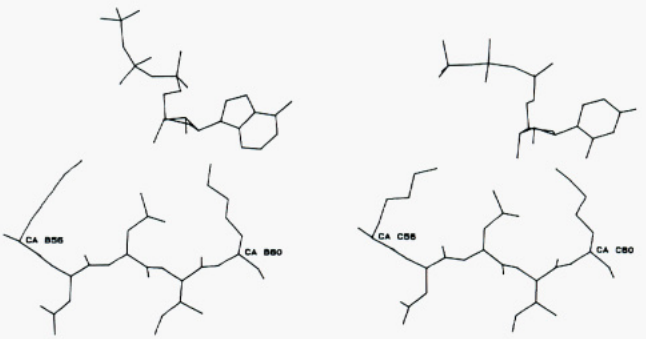

FIGURE 9: Illustration of regulatory residues Lys56 and Lys60 and their location with respect to the nucleotides ATP (left) and CTP (right). Both residues have been mutated to alanine. Lys56 → Ala becomes insensitive to ATP effects and Lys60 → Ala insensitive to CTP effects.

in part to discrimination between the two effectors. Although our studies of the T form were made at pH 5.8, where the detailed binding of the phosphate moieties may be different from that at higher pH, we do not expect to see a shift in the ring position if the pH is increased because of the limitations of the pocket in which they bind. Although pH effects may come in local conformations, the expansion of the molecule along the 3-fold axis as the T to R transition occurs is not noticeably affected by a change of pH from 5.8 to 8.5 (Altman et al., 1982).

Mutagenic research within the regulatory chain has been conducted on both the allosteric and zinc domains. Two mutations within the S3′ β-strand are of particular interest. Lys56r, located at the beginning of the S3′ strand, is found to be 4.8 Å from the ribose hydroxy O3′ of ATP AND 5.6 Å from the same ribose hydroxyl group of CTP. Mutation of Lys56r to alanine restores its cooperative character upon binding of CTP; however, the altered enzyme does not respond to ATP (Corder & Wild, 1989). We find that Lys56r is close to Gln8r, Asp19r–Pro22r, Leu46r–Leu48r, and Ser50r, although it does not bind directly to ATP or CTP. However, Lys56r interacts with several critical residues that may influence the binding of both ATP and CTP. For instance (Figure 8, middle), Val9r is observed to move into place for interactions with ATP; however, this movement is not found in the T^{ctp} structure. Thus, the interaction of Lys56r with residues near Val9r may enhance the transmission of conformational information upon binding of ATP. We turn now to Lys60r, which is found to make several interactions with the base and ribose rings of ATP and CTP; Lys60r has been mutated to an alanine (Zhang & Kantrowitz, 1989). In this mutant, ATP shows normal effects upon binding, but CTP has no effect. Lys60r, which is located at the end of the S3′ strand, interacts with several critical residues, namely, Val9r, Glu10r, Thr16r, Val17r, Ile42r, and Thr43r, and the effectors ATP and CTP. Although both mutations (at 56 and 60) are similar (Lys → Ala), they have opposite effects with respect to ATP and CTP. A schematic diagram of residues 56 and 60 of the regulatory chain is shown in Figure 9. Although we are not able to present a fuller interpretation, we appreciate how subtle the effects are which describe the allosteric control and the intricate network in which these residues are involved. The last mutation that we discuss within the allosteric site is Lys94r → Gln[4] (Zhang et al., 1988). We find that Lys94r interacts

[4] The notation we use to name a mutant enzyme consists of the wild-type amino acid followed by its numerical location in the sequence on the left of an arrow, and on the right of the arrow is the abbreviation of the new amino acid. For example, Arg 54 → Ala indicates that the arginine at position 54 was changed to an alanine.

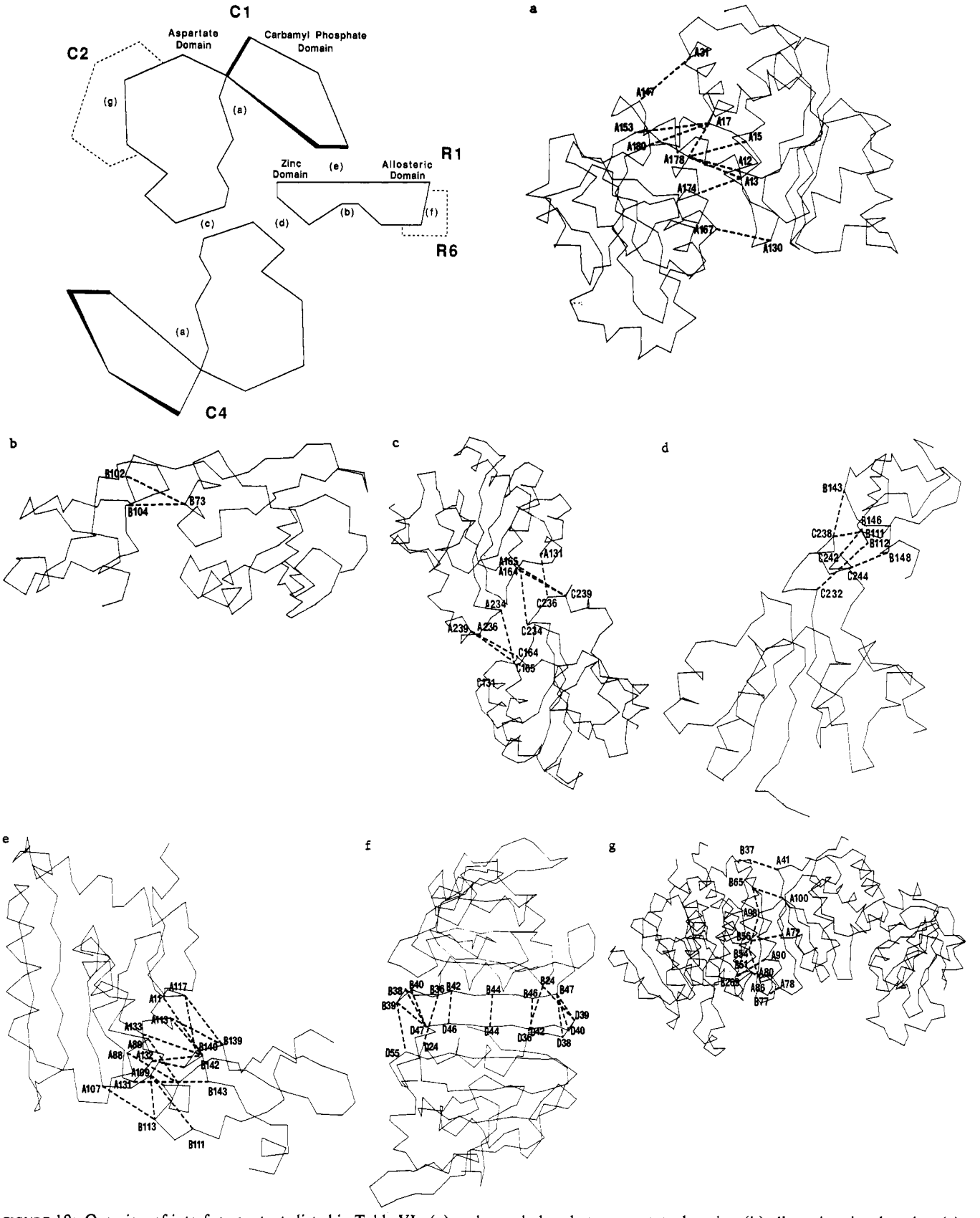

FIGURE 10: Overview of interface contacts listed in Table VI: (a) carbamoyl phosphate···aspartate domains; (b) allosteric···zinc domains; (c) C1···C4 chains; (d) aspartate···zinc domains; (e) carbamoyl phosphate···zinc domains; (f) R1···R6 chains; (g) C1···C2 interface. Residue numbering is based on the sequence reported in Ke et al. (1988). The A and C chains are C1,C6 catalytic chains, respectively; B and D chains are R1,R6 regulatory chains, respectively.

very closely with the phosphates of both ATP and CTP. The mutant enzyme is almost insensitive to ATP and shows a substantially reduced response to CTP. These results indicate that Lys94 is strongly involved in the binding of ATP and CTP. The only interactions of Lys94r occur with Thr82r–Asn84r. In general, caution is appropriate in interpretating the results of mutagenesis, especially in analyzing thermodynamic properties (Gao et al., 1989). The connection between

Table VI: Domain Interface Contacts[a] Illustrated in Figure 8 for T-State Aspartate Carbamoyltransferase

(a) CP···Asp	
Asn13 OD1···Gln174 NE2	Arg17 NE···Lys178 O
Ile12 O···Lys178 NZ	Arg17 NH1···Asp153 OD1
Asn13 O···Lys178 NZ	Arg17 NH2···Asp180 OD2
Leu15 O···Lys178 NZ	Lys31 NZ···Gln147 OE1
(b) All···Zn	
Gln73 NE2···Arg102 O	Gln73 OE1···Asp104 N
(c) c1···c4	
Lys164 NZ···Glu239 OE2	Glu234 O···Tyr165 OH
Tyr165 OH···Glu239 OE2	Glu239 OE1···Lys164 NZ
Ser131 OG···Asp236 OD1	Glu239 OE1···Tyr165 OH
(d) Asp···Zn	
Lys232 NZ···Ser112 OG	Ser238 OG···Lys143 NZ
Ser238 OG···Asn111 OD1	Asn242 OD1···Ser146 N
(e) CP···Zn	
Ser11 OG···Glu142 OE2	Arg113 NH2···Glu142 OE1
Leu88 N···Glu119 OE2	Glu117 OE2···Lys139 NZ
Ala89 N···Glu119 OE2	Glu117 OE1···Tyr140 OH
Pro107 O···Asn113 ND2	Ser131 OG···Lys143 NZ
Glu109 OE1···Asn111 ND2	Asn132 ND2···Cys141 O
Glu109 N···Asn113 O	Asn132 ND2···Glu142 OE1
Glu109 O···Ile115 N	Gln133 NE2···Glu142 OE2
Arg113 NH2···Lys139 O	
(f) r1···r6	
Gln24 NE2···Thr36 O	Ile42 O···Leu46 N
Gln24 NE2···Asp39 OD1	Ile44 O···Ile44 N
Thr36 O···Gln24 NE2	Leu46 N···Ile42 O
Thr38 O···Asn47 ND2	Asn47 ND2···Thr38 O
Asp39 O···Asn47 ND2	Asn47 ND2···Asp39 O
Asp39 O···Arg55 NH1	Asn47 ND2···Gln40 O
Gln40 O···Asn47 ND2	
(g) c1···c2	
His41 NE2···Glu37 OE2	Asp90 OD2···Arg269 NH2
Gly72 O···Lys56 NH1	Tyr98 OH···Arg54 O
Asn78 OD1···Ala77 N	Tyr98 O···Arg65 NH2
Ser80 OG···Ala51 O	Asp100 OD2···Arg65 NH1
Glu86 OE1···Arg54 NH1	

[a] Interface contacts are defined as contacts less than 3.5 Å capable of making an electron donor–acceptor pair. Key: CP, carbamoyl phosphate domain; Asp, aspartate domain; All, allosteric domain; Zn, zinc domain.

structure and thermodynamic quantities can be complex.

The concept that the binding of allosteric effectors modifies the equilibrium between the two forms of ATCase where these forms differ both in substrate affinity and in quaternary structure has been debated over the years (Changeaux & Rubin, 1968; Howlett et al., 1977; Thiry & Hervé, 1978; Tauc et al., 1982; Hervé et al., 1985). In our analysis, which was conducted without the presence of substrates and at a less than optimal pH, we observe that ATP alters the quaternary structure: ATP drives the T form in the direction of the R structural state. It has yet to be shown that these structural changes alter the equilibrium between the T and R forms. Illustrated in Figure 10 and listed in Table VI are the interface contacts between the enzyme domains, where no salt links or hydrogen bonds were found to be broken or created, although in the T^{atp} structure, many of the distances were found to be longer (0.3–0.5 Å) than in the corresponding unligated and T^{ctp} structures. Again, these longer contacts could facilitate the movement of the 240s loop when the second substrate (Asp) binds and may increase the affinity for aspartate.

Conditions need to be established under which these effectors can alter the T to R equilibrium, in view of the strong interactions of catalytic trimers in the T form and the strong binding of *N*-(phosphonoacetyl)-L-aspartate (Hervé et al., 1985). To this end we are examining structures in which ATP or CTP (or CTP/UTP) is bound to the Glu239 → Gln mutant, which in the crystal state occurs in an intermediate quaternary conformation (Gouaux et al., 1989); in this mutant the C1–C4 interface contacts are disrupted between Glu239 and the pair Lys164 and Tyr165 of the crystallographically related catalytic chain. This mutant is very sensitive to both CTP and carbamoyl phosphate. In preliminary structural studies, the CTP-complexed mutant is observed to draw the enzyme back into a structural T state as determined by unit cell determinations for the mutant enzyme (c = 174 Å) (Gouaux et al., 1989) versus the CTP-ligated mutant (c = 142 Å). Furthermore, X-ray solution scattering studies of the Gln239 mutant indicate that carbamoyl phosphate is able to complete the T → R transition. Furthermore, CTP returns the enzyme to the T state in the absence of carbamoyl phosphate and part of the way with carbamoyl phosphate (Tauc et al., 1990). Similarly, in the pAR5 mutant in which residues 145–153 of the regulatory chain have been replaced in the C1···R1 interface, an intermediate state structure has been observed with X-ray solution scattering (Cherfils et al., 1987). Upon addition of PALA, charbamoyl phosphate, or ATP, the enzyme is displaced toward the R state while CTP was found to have little effect upon the quaternary structure.

Lastly, in order to determine the nucleotide binding effects of the enzyme in the R state, the CTP- and ATP-ligated structures have been determined with the weakly bound substrates phosphonoacetamide/malonate in the active site. Independent of the T-state effector analysis, it was observed that ATP had little effect on the catalytic trimer separation, while CTP perturbed the allosteric transition in the direction of the T state by decreasing the catalytic trimer separation (–0.5 Å). These results suggest that the nucleotide regulators alter the catalytic efficiency by perturbing the allosteric transition. The R-state enzyme with nucleoside triphosphates is presented in the following paper, and a comparison of the T and R state with bound effectors will be published in the near future.

Added in Proof

In reference to Figure 10b we have found that Tyr77 of the allosteric domain is in close proximity to the zinc domain. Therefore, this residue may be important for communication between the allosteric and zinc domains.

Acknowledgments

We thank R. Kantrowitz and his colleagues at Boston College for large quantities of the enzyme aspartate carbamoyltransferase, R. Chandros, R. Kretsinger, T. Ptak, and S. Sobottka of the University of Viriginia for use of the MAXD system in the collection of X-ray diffraction data, and the Pittsburgh Supercomputing Center for the use of the Cray YMP, which allowed for rapid refinement. We also thank Dr. Hengming Ke for discussions regarding the manuscript, Charles Cho for assistance with the figures, and Y. M. Chook for carefully proofreading the manuscript.

Registry No. Aspartate carbamoyltransferase, 9012-49-1.

References

Altman, R. B., Ladner, J. E., & Lipscomb, W. N. (1982) *Biochem. Biophys. Res. Commun. 108*, 592–595.

Baillon, J., Tauc, P., & Hervé, G. (1985) *Biochemistry 24*, 7182–7187.

Beck, D., Kedzie, K. M., & Wild, J. R (1989) *J. Biol. Chem. 264*, 16629–16637.

Bethell, M. R., Smemh, K. E., Wheme, J. S., & Jones, M. E. (1968) *Proc. Natl. Acad. Sci. U.S.A. 60*, 1442–1449.

Brünger, A. T. (1988) *X-PLOR Manual*, version 1.5, Yale University, New Haven, CT.
Brünger, A. T., Kuriyan, J., & Karplus, M. (1987) *Science 235*, 458–460.
Changeux, J.-P., & Rubin, M. M. (1968) *Biochemistry 7*, 553–560.
Cherfils, J., Vachette, P., Tauc, P., & Janin, J. (1987) *EMBO J. 6*, 2843–2847.
Corder, T. S., & Wild, J. R. (1989) *J. Biol. Chem. 264*, 7425–7430.
Creighton, T. E. (1983) *Proteins—Structures and Molecular Principles*, pp 459–464, W. H. Freeman and Co., New York.
Foote, J., Lauritzen, A. M., & Lipscomb, W. N. (1985) *J. Biol. Chem. 260*, 9624–9629.
Fox, G. C., & Holmes, K. C. (1966) *Acta Crystallogr. 20*, 886–891.
Gao, J., Kuczera, K., Tidor, B., & Karplus, M. (1989) *Science 244*, 1069–1072.
Gerhart, J. C., & Pardee, A. B. (1962) *J. Biol. Chem. 237*, 891–896.
Gerhart, J. C., & Schachman, H. K. (1965) *Biochemistry 4*, 1054–1062.
Gouaux, J. E., & Lipscomb, W. N. (1988) *Proc. Natl. Acad. Sci. U.S.A. 85*, 4205–4208.
Gouaux, J. E., & Lipscomb, W. N. (1989) *Proc. Natl. Acad. Sci. U.S.A. 86*, 845–848.
Gouaux, J. E., & Lipscomb, W. N. (1990) *Biochemistry 29*, 389–402.
Gouaux, J. E., Krause, K. L., & Lipscomb, W. N. (1987) *Biochem. Biophys. Res. Commun. 142*, 893–897.
Gouaux, J. E., Stevens, R. C., Ke, H. K., & Lipscomb, W. N. (1989) *Proc. Natl. Acad. Sci. U.S.A. 86*, 8212–8216.
Hervé, G., Moody, M. F., Tauc, P., Vachette, P., & Jones, P. T. (1985) *J. Mol. Biol. 185*, 189–199.
Howlett, G. J., Blackburn, M. N., Compton, J. G., & Schachman, H. K. (1977) *Biochemistry 16*, 5091–5099.
Hsuanyu, Y., & Wedler, F. C. (1987) *Arch. Biochem. Biophys. 259*, 316–330.
Hsuanyu, Y., & Wedler, F. C. (1988) *J. Biol. Chem. 263*, 4172–4181.
Jones, M. E., Spector, L., & Lipmann, F. (1955) *J. Am. Chem. Soc. 77*, 819–820.
Kantrowitz, E. R., & Lipscomb, W. N. (1988) *Science 241*, 669–674.
Kantrowitz, E. R., & Lipscomb, W. N. (1990) *Trends Biochem. Sci. 15*, 53–59.
Ke, H. M., Honzatko, R. B., & Lipscomb, W. N. (1984) *Proc. Natl. Acad. Sci. U.S.A. 81*, 4037–4040.
Ke, H. M., Lipscomb, W. N., Cho, Y. J., & Honzatko, R. B. (1987) *J. Mol. Biol. 196*, 853–875.
Kennard, O., Isaacs. N. W., Motherwell, W. D. S., Coppola, J. C., Wampler, D. L., Larson, A. C., & Watson, D. G. (1971) *Proc. R. Soc. London, A 325*, 401–436.
Kim, K. H., Pan, Z., Honzatko, R. B., Ke, H. M., & Lipscomb, W. N. (1987) *J. Mol. Biol. 196*, 853–875.
Klinger, A. L., & Kretsinger, R. H. (1989) *J. Appl. Crystallogr. 22*, 287–293.
Krause, K. L., Volz, K. W., & Lipscomb, W. N. (1987) *J. Mol. Biol. 193*, 527–553.
Kuriyan, J., Karplus, M. K., & Petsko, G. (1987) *Proteins 2*, 1–12.
Luzzati, V. (1952) *Acta Crystallogr. 5*, 802–810.
Monod, J., Wyman, J., & Changeaux, J.-P. (1965) *J. Mol. Biol. 12*, 88–118.
Pfugrath, J., Saper, M. A., & Quiocho, F. A. (1984) *Methods and Applications in Crystallographic Computing* (Hall, S., & Ashiaka, T., Eds.) pp 404–407, Clarendon Press, Oxoford, U.K.
Philips, J. C., Bordas, J., Foote, A. M., Koch, M. H., & Moody, M. F. (1982) *Biochemistry 21*, 830–834.
Reichard, P., & Hanshoff, G. (1956) *Acta Chem. Scand. 10*, 548–566.
Sabottka, S. E., Cornick, G. G., Kretsinger, R. H., Rains, R. G., Stephens, W. A., & Weissman, L. J. (1984) *Nucl. Instrum. Methods 220*, 575–581.
Schachman, H. K. (1988) *J. Biol. Chem. 263*, 18583–18586.
Tauc, P., Leconte, C., Kerbiriou, D., Thiry, L., & Hervé, G. (1982) *J. Mol. Biol. 155*, 155–168.
Tauc, P., Vachette, P., Middleton, S. A., & Kantrowtiz, E. R. (1990) *J. Mol. Biol.* (in press).
Thiry, L., & Hervé, G. (1978) *J. Mol. Biol. 125*, 515–534.
Tondre, C., & Hammes, G. G. (1974) *Biochemistry 13*, 3131–3136.
Weber, K. (1968) *Nature (London) 218*, 1116–1119.
Werner, W. E., & Schachman, H. K. (1989) *J. Mol. Biol. 206*, 221–230.
Wild, J. R, Johnson, J. L., & Loughrey-Chen, S. J. (1988) *J. Bacteriol. 170*, 446–448.
Wild, J. R., Loughrey-Chen, S. J., & Corder, T. S. (1989) *Proc. Natl. Acad. Sci. U.S.A. 86*, 46–50.
Wiley, D. C., & Lipscomb, W. N. (1968) *Nature (London) 218*, 1119–1121.
Zhang, Y., & Kantrowitz, E. R. (1989) *Biochemistry 28*, 7313–7318.
Zhang, Y., Ladjimi, M. M., & Kantrowitz, E. R. (1988) *J. Biol. Chem. 263*, 1320–1324.